Low frequency spectral modifications of seismic background noise due to interaction with oscillating fluids entrapped in porous rocks

Marcel Frehner (*), Department of Earth Sciences, ETH Zurich, Switzerland, +41 44 632 88 72, frehner@erdw.ethz.ch
Stefan M. Schmalholz, Department of Earth Sciences, ETH Zurich, Switzerland
Yuri Podladchikov, Physics of Geological Processes (PGP), University of Oslo, Norway

Abstract

In recent years a new method for direct hydrocarbon indication was developed. Studies of passive seismic data in the frequency range below 20Hz have shown that the frequency content of the ever-present geoseismic background noise changes above hydrocarbon reservoirs. Different explanations for this observation have been proposed. In this study, the effect of oscillating pore fluids on the background noise is investigated. A non-wetting fluid drop entrapped in a pore can oscillate with a characteristic eigenfrequency. Capillary forces act as the restoring force driving the oscillations. A 1D wave equation is coupled with a linear oscillator equation, which represents these pore fluid oscillations. The resulting linear system of equations is solved numerically with explicit finite differences. The most energetic part of the seismic background noise, i.e frequencies around 0.1-0.3Hz are used as the external source. This part is presumably related to seismic surface waves generated by ocean waves. It is shown that the resulting elastic wave initiates oscillation of the pore fluid The oscillatory energy of the fluid drops is transferred continuously to the elastic rock matrix. In consequence the elastic matrix carries a second frequency, the eigenfrequency of the pore fluid oscillation on top of the applied external frequency. The presented model is considered as a possible explanation for the observed spectral modifications above hydrocarbon reservoirs. Time evolution of the pore fluid oscillation seems to be related to the thickness of the hydrocarbon reservoir.

Introduction

Spectral modifications of seismic background noise in the low frequency range have been observed in nature above hydrocarbon-bearing structures (Bloch and Akrawi, 2006; Dangel et al., 2003). A new method for direct hydrocarbon indication was developed using spectra of passive seismic measurements. The physical explanation for these modifications is the subject of current discussions (Graf et al., 2007). Seismic attenuation phenomena in poro-elastic media, reflection patterns in the subsurface, and phase transition effects (Suntsov et al., 2006) were discussed recently as possible causes.

The behavior of non-wetting fluids entrapped in capillary tubes and in idealized pore spaces were thoroughly studied in the past (Dvorkin et al., 1990; Graham and Higdon, 2000a, 2000b). The main finding of these studies is the oscillatory movement of fluids when an external force is applied. The frequencies of these oscillations can be reasonably low. The driving force is the surface tension force acting on the interface between the wetting and the non-wetting fluid phase. The results of these works were used by the oil and gas industry to develop a new enhanced oil recovery (EOR) method termed "wave stimulation of oil" or "vibratory mobilization" (Beresnev et al., 2005; Iassonov and Beresnev, 2003; Li et al., 2005). The general idea of the method is to excite oscillations of the entrapped oil with a vibratory device. Inertial forces occurring with oscillations eventually are strong enough to overcome the capillary pressure. This way the oil drops are enabled to leave the pore constrictions. The method and many application results are reviewed in Beresnev and Johnson, 1994. Biot, 1962 and many following publications consider fully saturated porous rocks where no oscillations can take place. The main focus of these publications is to better understand the dynamics of the second or slow P-wave that is special feature of Biot's poro-elastic theory. The work presented here focuses on the effect of low frequency pore fluid oscillations on seismic waves traveling through a porous rock. Such oscillations only occur in partially saturated rocks. Naturally induced oscillations are considered that are generated by the ever present seismic background noise. A one-dimensional two phase model is introduced that describes the coupling between elastic wave propagation and the oscillatory movement of the fluid.

Methods

Pore fluid oscillations as linear oscillations

Various theoretical investigations showed that a non-wetting fluid drop, i.e. oil, entrapped in a capillary tube can oscillate (Beresnev, 2006; Graham and Higdon, 2000a, 2000b; Hilpert et al., 2000). Both sliding and pinned contact lines were considered. In both cases the radii of the menisci change when the fluid drop is displaced out of its equilibrium position. In the case of sliding contact lines a variable width of the capillary tube has to be assumed to obtain the change of radii. This change of radii of the menisci changes the capillary pressure at the corresponding menisci which leads to a restoring force that drives the oscillation. Hilpert et al., 2000 demonstrated a resonant behavior of such oscillations and Holzner et al., 2007 showed that possible eigenfrequencies range down to reasonably low values

(<10Hz). For simplicity, oscillations of pore fluids in this work are approximated with a linear one-dimensional oscillator model with the eigenfrequency ω_0.

$$\ddot{u}^f = -\omega_0^2 u^f \qquad (1)$$

Superscript f indicates that it is a fluid that oscillates in the pores. u^f is the displacement of the fluid and $\ddot{u}^f$ is the second time derivative of the displacement, i.e. the acceleration. Considering n such oscillators the total kinetic energy of the fluid E_{kin}^f is

$$E_{kin}^f = \frac{1}{2}\sum_{i=1}^{n} m_i^f \left(\dot{u}_i^f\right)^2 \qquad (2)$$

m_i^f is the mass of each individual oscillator and $\dot{u}^f$ is the time derivative of the displacement of each oscillator, i.e. the velocity. Assuming non-connected pores (i.e. the oscillations do not interact) the total potential energy E_{pot}^f consists of the sum of the individual potential energies. The eigenfrequency of the oscillations are here assumed to be constant for all pores.

$$E_{pot}^f = \frac{1}{2}\sum_{i=1}^{n} m_i^f \omega_0^2 \left(u_i^f\right)^2 \qquad (3)$$

Coupling between pore fluid oscillations and elastic wave

The pore fluid oscillations are coupled to a one-dimensional linear elastic solid. A sketch of the rheological model is given in Figure 1. The beam on the right hand side represents a one dimensional linear elastic solid which is coupled to a one dimensional linear oscillator (left hand side). The oscillations influence the behaviour of the elastic solid and vice versa. A detailed description of the coupling between solid and fluid subsystems is given in the Appendix. In the continuous limit of an infinite number of pore fluid oscillators the total kinetic energies E_{kin} and total potential energies E_{pot} of the fluid and solid subsystems is given by

$$
\begin{aligned}
E_{kin}^f &= \frac{1}{2}\int_0^l S\phi\rho^f \left(\dot{u}^f\right)^2 dx \\
E_{pot}^f &= \frac{1}{2}\int_0^l S\phi\rho^f \omega_0^2 \left(u^f - u^s\right)^2 dx \\
E_{kin}^s &= \frac{1}{2}\int_0^l (1-\phi)\rho^s \left(\dot{u}^s\right)^2 dx \\
E_{pot}^s &= \frac{1}{2}\int_0^l \sigma^s \varepsilon^s dx
\end{aligned}
\qquad (4)
$$

Superscript s denotes the solid part of the system. The discrete function u^f and its time derivatives (Equation (2) and (3)) become continuous functions. l is the total length of the one-dimensional model. ϕ is porosity of the elastic rock and ρ^f and ρ^s is fluid and solid mass density, respectively. S the filling level of the pores and is a number between 0 and 1. σ^s is the stress in the elastic rock and ε^s is the strain, i.e. spatial derivative of solid displacement. In the elastic solid subsystem stress is

related to strain with Young's modulus as the factor of proportionality.

$$\sigma^s = E\varepsilon^s = E\frac{\partial u^s}{\partial x} \qquad (5)$$

Equations (4) only consider the solid and fluid subsystems. When the filling level of the pores S is smaller than 1, a third phase is present in the system. Here it is assumed to be a gaseous phase. Both its kinetic and potential energy is small compared to the fluid and solid phases and is neglected. For the continuous two-component system Hamilton's variational principle can be applied to the Lagrangian functional L (Fetter and Walecka, 1980).

$$\delta\int_{t_1}^{t_2} L dt = \delta\int_{t_1}^{t_2}(T-U)dt = \int_{t_1}^{t_2}\int_0^l \delta\mathcal{L}dxdt \qquad (6)$$

T and U are the total kinetic energy ($E_{kin}^f + E_{kin}^s$) and the total potential energy ($E_{pot}^f + E_{pot}^s$) of the coupled system, respectively. t_1 and t_2 are two points in time. $\mathcal{L}$ is the Lagrangian density and has the dimension of energy per unit length. Using correct boundary conditions for the variation in space and time and assuming small variations, Equation (6) splits into two equations for the solid and fluid.

$$\delta\int_{t_1}^{t_2} L dt = \int_{t_1}^{t_2}\int_0^l \left\{\frac{\partial\mathcal{L}}{\partial u^i}\delta u^i + \frac{\partial\mathcal{L}}{\partial\dot{u}^i}\delta\dot{u}^i + \frac{\partial\mathcal{L}}{\partial\varepsilon^i}\delta\varepsilon^i\right\}dxdt = 0 \qquad (7)$$

Superscript i replaces superscript s (solid) or f (fluid). Integration by parts is carried out omitting the resulting boundary terms. Variations δu^i arise as common multipliers for all terms. Since the variations are arbitrary, the remaining terms have to be equal to zero. The resulting equations are the Euler-Lagrange equations for the continuous two-component system.

$$\frac{\partial\mathcal{L}}{\partial u^i} - \frac{\partial}{dt}\left(\frac{\partial\mathcal{L}}{\partial\dot{u}^i}\right) - \frac{\partial}{dx}\left(\frac{\partial\mathcal{L}}{\partial\varepsilon^i}\right) = 0 \qquad (8)$$

The Lagrangian density $\mathcal{L}$ (Equation (6)) is substituted into the Euler-Lagrange equations. The final equations of motion result.

$$
\begin{aligned}
S\phi\rho^f \frac{\partial^2 u^f}{\partial t^2} &= -S\phi\rho^f \omega_0^2\left(u^f - u^s\right) \\
(1-\phi)\rho^s \frac{\partial^2 u^s}{\partial t^2} &= \frac{\partial}{\partial x}\left(E\frac{\partial u^s}{\partial x}\right) + S\phi\rho^f \omega_0^2\left(u^f - u^s\right)
\end{aligned}
\qquad (9)
$$

First Equation (9) is almost identical to a linear one-dimensional oscillator equation (Equation (1)). It differs in the sense of its formulation in terms of relative displacement and averaged density ($S\phi\rho^f$). The left hand side together with the first term of the right hand side of the second Equation (9) is similar to a one-dimensional wave equation (Szabo, 1956). It is also written in terms of the averaged density (($1-\phi)\rho^s$). The additional term on the right hand side is also written in terms of relative displacement and links the fluid and the solid motion.
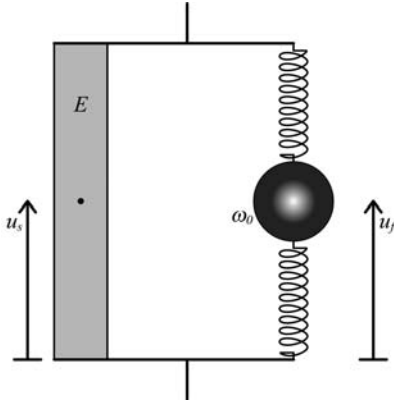
Figure 1: Schematic rheological model for the coupling between elastic deformation and pore fluid oscillations. The elastic bar with Young's modulus E on the left hand side is coupled with a linear oscillator with an eigenfrequency of ω_0. Two displacements have to be considered individually in this model, the displacement of the elastic subsystem u_s and the displacement of the oscillatory fluid subsystem u_f.

Numerical methods and setup

Using Equation (5) and two kinematic equations for u^f and u^s Equations (9) can be expanded to five first order linear partial differential equations. They are discretized using the finite difference method on a one-dimensional staggered grid (Virieux, 1986). Discretization in time is formulated explicitly with a predictor-corrector method. Boundary conditions can be rigid (all velocities equal Zero) or non-reflecting (Ionescu and Igel, 2003). The model setup used for the first set of simulations is shown in Figure 2a). Three receivers are placed in a homogeneous two-component model that is described by Equations (5) and (9). An external source can be applied at the position of receiver R_1. The source affects the solid matrix directly. The fluid phase is only affected indirectly through the coupling terms in Equations (9). The second Equation (9) becomes

$$(1-\phi)\rho^s \frac{\partial^2 u^s}{\partial t^2} = \frac{\partial}{\partial x}\left(E \frac{\partial u^s}{\partial x}\right) + S\phi\rho^f \omega_0^2 \left(u^f - u^s\right) + F \quad (10)$$

The Fourier spectrum of a typical measurement of ambient seismic noise shows a very distinct peak at around 0.1-0.3Hz (left gray bar in Figure 9). This high energy spectral peak is a global feature that can be measured everywhere in the world. It is presumably related to seismic surface waves generated by ocean waves (Aki and Richards, 1980). In this study the seismic background noise is reduced to this dominant peak. The external source term in Equation (10) becomes

$$F = F(x,t) = A_0(x)\sin(\Omega t) \quad (11)$$

with
$$\begin{aligned} A_0(x) &= 0 \qquad for\ x \neq x_{source} \\ A_0(x) &= 1 \qquad for\ x = x_{source} \end{aligned} \quad (12)$$

$\Omega = 1.89$ (= 0.3Hz · 2π). The external source is applied only at one point x_{source} in the model domain. The

eigenfrequency of the pore fluid oscillations is fixed to 3Hz throughout the model domain according to Holzner et al., 2007. Physical parameters used in the simulations are given in Table 1.
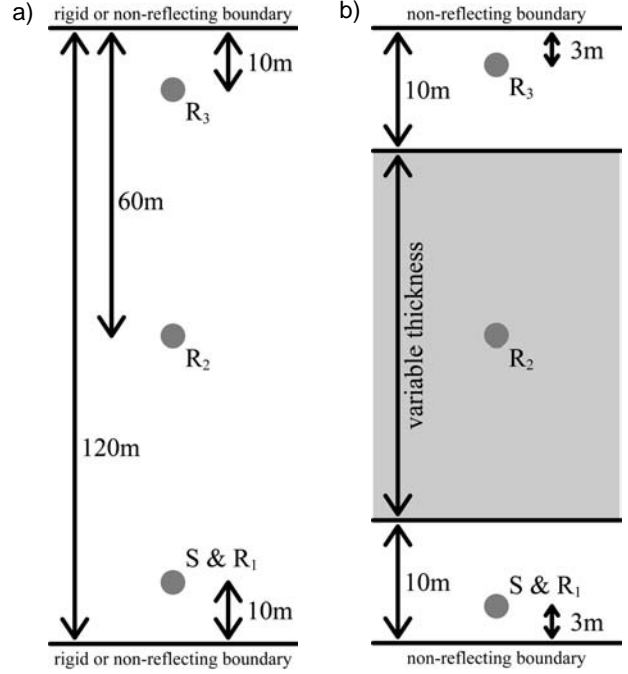
Figure 2: a) Homogeneous 1D model setup for numerical simulations consists of three receivers R_1-R_3 and one source S. The position of the source is identical with the position of receiver R_1. The whole system is described by the coupled system of Equations (9). The lower and upper boundaries can be rigid (zero displacement) or non-reflecting. b) Layered 1D model setup. The middle layer is described by the coupled system of Equations (9), the upper and lower layers are linear elastic. The lower and upper boundaries are non-reflecting.

| Symbol	Value
ω_0	18.85 (=3Hz · 2π)
ρ^f	800 kg m^{-3}
ρ^s	2800 kg m^{-3}
E	$2 \cdot 10^{10}$Pa
ϕ	0.3
S	0.9
Ω	1.89 (=0.3Hz · 2π)

Table 1: Parameters used in numerical simulations. Parameters not listed in this table are explained in the text.

Numerical results

Energy conservation and transfer

The introduced model is run with the setup shown in Figure 2a) with two rigid boundaries. No source is applied, but a Gaussian bell curve in space is used as the initial condition of the solid velocity. The four energies in the system, Equations (4) are calculated. Figure 3 shows the time evolution of the four energies (thin lines). Also, the total fluid energy and the total solid energy are shown

together with the total energy of the system (thick lines). The energies of the solid and fluid phase of the system always add up to constant total system energy, i.e. the total energy is conserved. At the same time energy is transferred back and forth between the solid and the fluid subsystem. The beginning with zero energy of the fluid represents the initial conditions. That the oscillations of the different energy contributions over time happen with similar amplitudes shows that the pore fluid oscillations influence the behavior of the solid phase considerably.
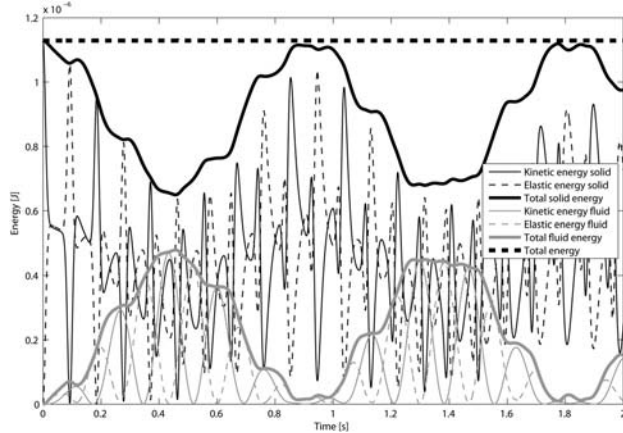

Figure 3: Time evolution of the four different energies in the system. The total energy, i.e. the sum of all energies (thick dashed line) stays constant over time. Individual energy contributions are transferred between fluid (gray lines) and solid (black lines) subsystems.

Homogeneous simulations

Numerical simulations are run for 120 seconds physical time with the model setup shown in Figure 2a) with two non-reflecting boundary conditions and the external source applied to the solid phase. At all three receiver positions the Fourier spectrum of the recorded solid velocity is calculated and plotted in Figure 4. They all show a very distinct peak at the frequency of the external force at 0.3Hz, as expected. The applied wave travels through the model domain with a constant frequency. In addition a second peak appears in all three spectra at 3 Hz. It coincides with the eigenfrequency of the pore fluid oscillations ω_0. This indicates that the elastic wave excites the pore fluid oscillations whose movements are indeed transferred back to the elastic matrix. This transfer is strong enough that the corresponding frequency peak is carried on top of the externally applied frequency Ω. Both frequencies can be measured in the solid velocity signal at any point of the model domain. The trough of the spectra at receiver R_1 (black spectra) is an artifact of the fast Fourier transform (FFT) and has no physical meaning. Figure 5 illustrates the second frequency that is carried on top of the external frequency. Figure 5a) shows a short time interval of the velocity measurement at receiver R_2. The fluid velocity (dashed grey line) seems to be identical to the solid velocity (solid black line). The difference between the two velocities is shown in Figure 5b). It is clear that they are not identical. The difference is characterized by the eigenfrequency of the pore fluid

oscillations. This frequency is measurable and appears in the Fourier spectrum (Figure 4). For ongoing physical time the Fourier spectrum changes. Figure 6 shows the time evolution of the Amplitudes of both peaks in the spectrum (0.3Hz: gray line, 3Hz: black line). The peak at 0.3Hz in the spectrum stays constant over time. On the other hand the peak at 3Hz decreases over time.
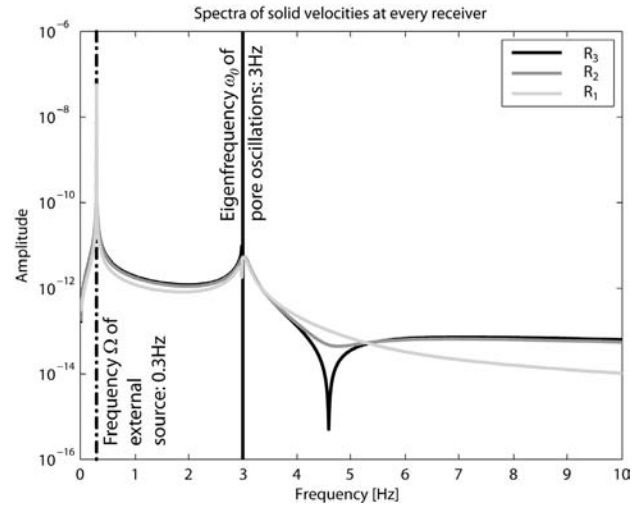

Figure 4: Fourier spectra of solid velocity time signals for three receivers R_1-R_3 (Figure 2a) after 120 seconds physical time. Two non-reflecting boundary conditions and sinusoidal external source acting on the solid phase at position S are applied. Dash-dotted vertical line: Frequency of external force (0.3Hz); Solid vertical line: Eigenfrequency of pore fluid oscillations (3Hz). The trough around 4.6Hz in the spectra of receivers R_2 and R_3 is an artefact of the fast Fourier transformation and has no physical meaning.
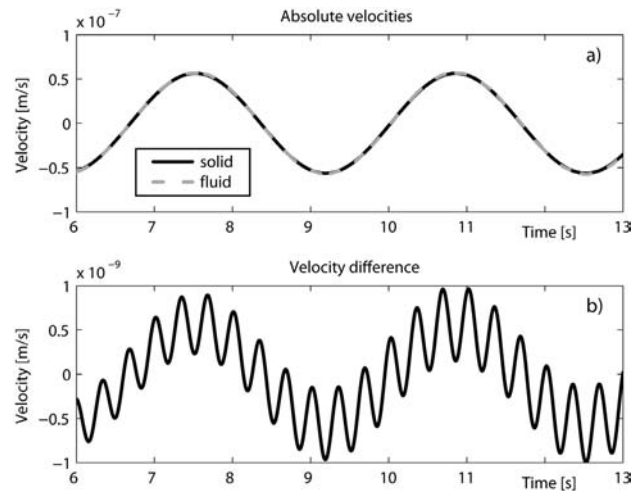

Figure 5: a) Section of time signals of absolute fluid (dashed grey line) and solid (solid black line) velocities recorded at receiver R_2. b) Same section of time signal of the difference between fluid and solid velocity. The difference between the two signals shows the eigenfrequency of the pore fluid oscillations (ω_0 = 3Hz) and the frequency of the external source (Ω = 0.3Hz).

Layered media

In a second set of numerical simulations the model setup was changed according to Figure 2b). Below and on top of the homogeneous model a purely elastic layer is added. This model setup allows the external source and receiver R_1 and R_3 to be outside the porous medium. Since the model is one-dimensional and the additional layers are linear elastic, neither the distance of receivers R_1 and R_3 from the porous layer nor the distance of the source S from the porous layer change the recorded signal. They only add a time shift to the signal without changing its character. No change in the Fourier spectrum is expected. Therefore the distance of receivers R_1 and R_3 from the porous layer and the distance of the source S from the porous layer are chosen to be small (7m) to optimize the numerical resolution. Several numerical simulations with different thicknesses of the porous layer were performed. At receiver R_3 a Fourier spectrum is calculated out of the recorded solid velocity after different simulation lengths. Figure 7 shows the evolving Fourier spectrum for the case of a 50m thick porous layer. As in the homogeneous case (Figure 4) the amplitude of the peak at 0.3Hz stays constant over time while the amplitudes of all other frequencies, including 3Hz, decrease. This decrease of the spectral amplitude at the eigenfrequency of the pore fluid oscillations is different for different thicknesses of the porous layer. Figure 8 shows the time evolution of the ratio between the spectral amplitudes of the 3Hz-peak and the 0.3Hz-peak. A thick porous layer initially creates higher amplitudes of the spectral peak at 3Hz. This amplitude decreases linearly with time on double-logarithmic axes. A thin porous layer initially creates lower amplitudes of the spectral peak at 3Hz. The decrease with time is smaller until the amplitude asymptotically reaches the values for thicker layers. A saturation of this effect occurs at a thickness of the porous layer of around 70m.
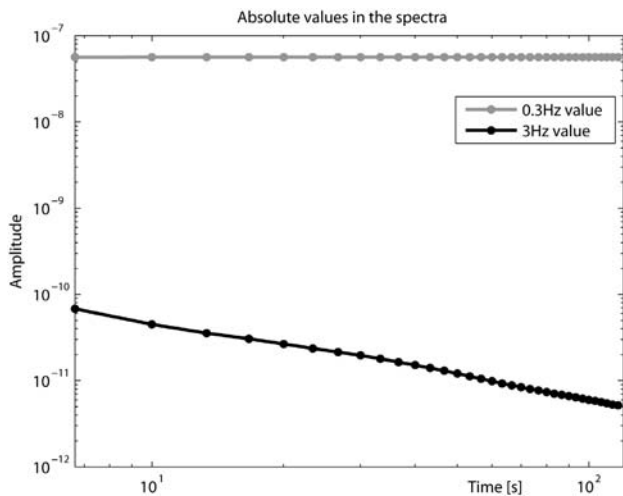
Figure 6: Double logarithmic representation of time evolution of the spectral peaks at 0.3Hz (gray line) and 3Hz (black line). The spectra are calculated after different simulation lengths with the solid velocity time signal at receiver R_2. While the 0.3Hz-peak stays constant over time the 3Hz-peak decreases in amplitude.
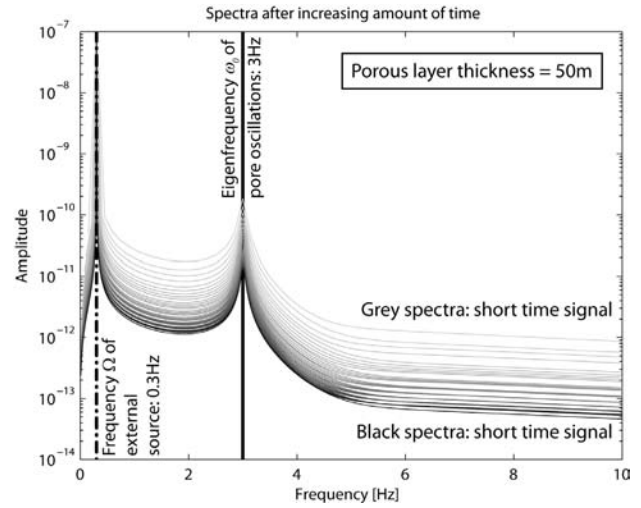
Figure 7: Spectra of solid velocity time signal at receiver R_3 of the layered model for a porous layer thickness of 50m. Different spectra are calculated after different simulation lengths with gray spectra representing short simulations. Longest time signal is 120s, shortest is 3.5s. Dash-dotted vertical line: Frequency of external force; Solid vertical line: Eigenfrequency of pore fluid oscillations.
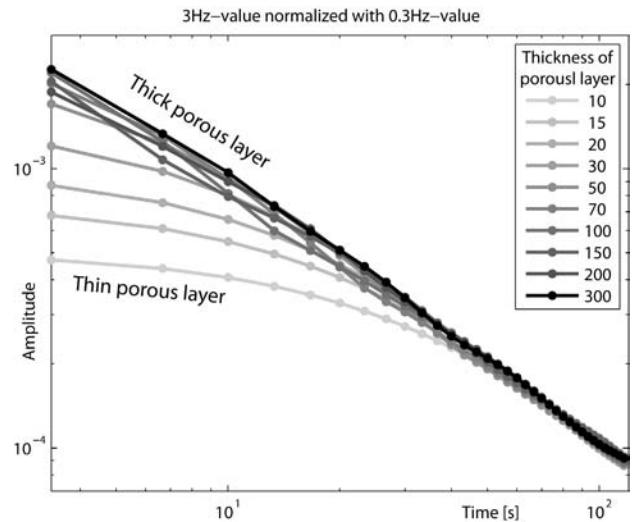

Figure 8: Double-logarithmic representation of time evolution of the amplitude ratio between the 3Hz-peak and the 0.3Hz-peak in the spectra. Different colors represent different porous layer thicknesses with thinner porous layers as gray curves. Spectra are calculated with the solid velocity time signal at receiver R_3 of the layered model.

Discussion and Conclusions

The introduced Equations (9) to model the coupling between pore fluid oscillations and elastic wave propagation are linear. Still, the monochromatic external source (Equation (11)) acting on the solid phase excites the pore fluid to oscillate with its eigenfrequency. These

oscillations are initiated by the incident of the elastic wave. While the wave itself is monochromatic, the wave front contains all frequencies, including the eigenfrequency of the pore fluid oscillations. After the wave front has passed, the pore fluid continues to oscillate with its eigenfrequency ω_0 and constantly transfers energy to the elastic porous matrix. This results in a decrease of the amplitude of the oscillations. The energy transfer from the oscillating pore fluid to the elastic solid matrix is strong enough to change the frequency content of the elastic wave. Similar modifications of the seismic background noise have been observed above hydrocarbon-bearing structures (right gray bar in Figure 9). Oscillation of oil entrapped in pore constrictions must be considered as a possible explanation for these spectral modifications.
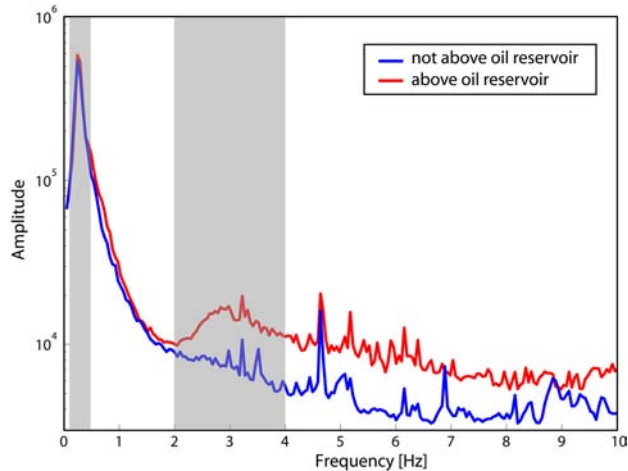
Figure 9: Field measurements of seismic background noise. One measurement above (red) and one nearby (blue) a proven oil reservoir. Source: Spectraseis survey for Petrobras, Potiguar Basin, Brazil, 2004

Acknowledgements

References

Aki, K. and Richards, P. G., 1980, Quantitative Seismology: Theory and Methods: W. H. Freeman and Company, ISBN 0-7167-1058-7

Beresnev, I. A., 2006, Theory of vibratory mobilization on nonwetting fluids entrapped in pore constrictions: Geophysics, **71**, N47-N56

Beresnev, I. A. and Johnson, P. A., 1994, Elastic-Wave Stimulation of Oil Production - a Review of Methods and Results: Geophysics, **59**, 1000-1017

Beresnev, I. A., Vigil, R. D., Li, W. Q., Pennington, W. D., Turpening, R. M., Iassonov, P. P. and Ewing, R. P.,

2005, Elastic waves push organic fluids from reservoir rock: Geophysical Research Letters, **32**,

Biot, M. A., 1962, Mechanics Of Deformation And Acoustic Propagation In Porous Media: Journal Of Applied Physics, **33**, 1482-1498

Bloch, G. and Akrawi, K., 2006, Application of Low Frequency Passive Seismic Surveys in ADCO, UAE: EAGE Workshop Passive Seismic, December 10-13, Dubai, United Arab Emirates

Courant, H. and Hilbert, D., 1993, Methoden der mathematischen Physik: Springer-Verlag, ISBN 3-540-04178-8

Dangel, S., Schaepman, M. E., Stoll, E. P., Carniel, R., Barzandji, O., Rode, E. D. and Singer, J. M., 2003, Phenomenology of tremor-like signals observed over hydrocarbon reservoirs: Journal Of Volcanology And Geothermal Research, **128**, 135-158

Dvorkin, J., Mavko, G. and Nur, A., 1990, The oscillations of a viscous compressible fluid in an arbitrarily-shaped pore: Mechanics of Materials, **9**, 165-179

Fetter, A. L. and Walecka, J. D., 1980, Theoretical mechanics of particles and continua: McGraw-Hill Book Company, ISBN 0-07-020658-9

Graf, R., Schmalholz, S. M., Podladchikov, Y. and Saenger, E., 2007, Passive low frequency spectral analysis: Exploring a new field in geophysics: World Oil, **January**, 47-52

Graham, D. R. and Higdon, J. J. L., 2000a, Oscillatory flow of droplets in capillary tubes. Part 1. Straight tubes: Journal of Fluid Mechanics, **425**, 31-53

Graham, D. R. and Higdon, J. J. L., 2000b, Oscillatory flow of droplets in capillary tubes. Part 2. Constricted tubes: Journal of Fluid Mechanics, **425**, 55-77

Hilpert, M., Jirka, G. H. and Plate, E. J., 2000, Capillarity-induced resonance of oil blobs in capillary tubes and porous media: Geophysics, **65**, 874-883

Holzner, R., Eschle, P., Dangel, S., Frehner, M., Narayanan, C. and Lakehal, D., 2007, Hydrocarbon microtremors interpreted as nonlinear oscillations driven by oceanic background waves: Communications in nonlinear science and numerical simulation, **topical issue "Geophysics"**, In Press

Iassonov, P. P. and Beresnev, I. A., 2003, A model for enhanced fluid percolation in porous media by application of low-frequency elastic waves: Journal of Geophysical Research-Solid Earth, **108**,

Li, W. Q., Vigil, R. D., Beresnev, I. A., Iassonov, P. and Ewing, R., 2005, Vibration-induced mobilization of trapped oil ganglia in porous media: Experimental validation of a capillary-physics mechanism: Journal of Colloid and Interface Science, **289**, 193-199

Suntsov, A. E., Aroutunov, S. L., Mekhnin, A. M. and Meltchouk, B. Y., 2006, Passive Infra-Frequency Microseismic Technology – Experience and Problems of Practical Use: EAGE Workshop Passive Seismic, December 10-13, Dubai, United Arab Emirates

Szabo, I., 1956, Höhere Technische Mechanik: Springer-Verlag, ISBN 3-540-15007-2

Virieux, J., 1986, P-Sv-Wave Propagation In Heterogeneous Media - Velocity-Stress Finite-Difference Method: Geophysics, **51**, 889-901